Electronic Supplementary Material (ESI) for Journal of Materials Chemistry A.

Supporting Information

A Cellulose-Complexing Strategy Induced Surface Regulation towards Ultrahigh Utilization Rate of Zn

Xin Li[a], Hong Yao[a], Yuhang Li[a], Xiangjie Liu[a], Du Yuan[a,*], Yingqian Chen[b], Ming Wah Wong[b], Yizhou Zhang[c,*] Haitao Zhang[d,*]

Experimental Methods

Synthesis of Electrolytes

The ZCEs were prepared by first mixing $ZnCl_2$ (6.815 g, 99.99%, Alfa Aesar, pre-dried in vacuum oven) with D. I. H_2O with a molar ratio of 1:2.2 under stirring at 75 °C until the transparent liquid was formed, followed by adding certain amount of cellulose (α-cellulose, C804600, Shanghai Macklin Biochemical Co., Ltd.) or tissue paper (0.2g, 0.6g, 1.0g) and continuous stirring until transparent.

Fabrication of artificial SEI on Zn

Galvanostatic charging method was applied on commercial Zn foil (99.99 %, 0.1 and 0.2 μm, Guantai metal material Co., Ltd), at 10 mA cm^{-2} for a certain deposition time, e.g., 1 to 3 h. After treatment, the Zn foil was washed with DI water and soaked in DI water, then dried at 60°C in vacuum oven for overnight. The samples were labelled as Zn-ZCE-x-yh, where x corresponds to the label for ZCEs, and y represents the duration in hours.

Material Characterizations

X-ray diffraction (XRD) were collected on a Bruker D8 Advance A25 X with Cu K_α irradiation (λ=1.5418 Å). The Fourier transform infrared spectroscopy (FTIR-ATR) was recorded by Shimadzu Instrument IRTracer-10 with the attenuated total reflectance compartment. Scanning electron microscopy (SEM) images and energy dispersive X-ray spectra (EDX) of the electrode were collected on a JSM-7900F. XPS spectra were collected by Kratos AXIS Supra XPS with dual anode (Al/Ag Kα) X-ray monochromatic source.

DFT calculations

DFT calculations for clusters $[Zn(OH_2)_n]^{2+} \cdot 2Cellulose$ were performed using Gaussian16,[1] to investigate the coordination between $[Zn(OH_2)_n]^{2+}$ and $Cellulose$. Specifically, all molecular geometries were optimized using the M06-2X functional with 6-31+g(d,p) basis set.[2] And frequency calculations were performed to verify the optimized minima.

The formation energy E_f of clusters was computed as below:

$$E_f = E\left([Zn(OH_2)_n]^{2+} \cdot 2Cellulose\right) - nE(H_2O) - E(Zn^{2+}) - 2E(Cellulose),$$

where $E\left([Zn(OH_2)_n]^{2+} \cdot 2Cellulose\right)$, $E(H_2O)$, $E(Zn^{2+})$, and $E(Cellulose)$ denote the total energy of $[Zn(OH_2)_n]^{2+} \cdot 2Cellulose$, H_2O, Zn^{2+}, and $Cellulose$, respectively.

The formation energies E_f were used to plot the convex hull *vs.* the number of H_2O (n),

which indicates the stable phases of clusters with increasing number of H_2O. As shown by the dashed line in Figure S2, n=1,4,5,6 are stable phases with a flattened slop to the next point in comparison with that to the previous one.

The charge density difference is calculated as:

$$\Delta\rho = \rho\left([Zn(OH_2)_n]^{2+} \cdot 2Cellulose\right) - \rho\left([Zn(OH_2)_n]^{2+}\right) - \rho(2Cellulose),$$

where $\rho\left([Zn(OH_2)_n]^{2+} \cdot 2Cellulose\right)$, $\rho\left([Zn(OH_2)_n]^{2+}\right)$, and $\rho(2Cellulose)$ correspond to electron density of $[Zn(OH_2)_n]^{2+} \cdot 2Cellulose$, $[Zn(OH_2)_n]^{2+}$, and $2Cellulose$, respectively. Specifically, the geometries of $[Zn(OH_2)_n]^{2+}$ and $2Cellulose$ were taken from the geometry of $[Zn(OH_2)_n]^{2+} \cdot 2Cellulose$.

Electrochemical characterizations

Linear sweep voltammetry (LSV) and cyclic voltammetry (CV) were carried out to determine the EWs of electrolytes by DH 7000 (Jiangsu Donghua Analytical Instrument Co., Ltd.) in a two-electrode cell with Pt foil as the work electrode, Zn foil as the counter electrode, at a scan rate of 1 mV·s^{-1}. Tafel curves were conducted in a 3-electrode configuration, with commercial Zn foil or ZCE-Zn as the working electrode, leakless type Ag/AgCl as the reference electrode, and Pt as the counter electrode, using the electrolytes of ZCEs or 2M $Zn(OTf)_2$ aqueous solution by commercial $Zn(OTf)_2$ (98 %, Sigma-Aldrich). The electrochemical impedance spectroscopy (EIS) measurements were carried out on DH 7000 electrochemical workstation in a frequency ranging from 0.1 Hz to 1.0 MHz with an AC amplitude of 1 mV. The ionic conductivities of electrolytes were measured by FE38 conductivity meter (Mettler Toledo). To calculate the transference number, current-time curve of Zn|Zn symmetric cell with electrolytes were measured after a constant potential of 10 mV. EIS spectra were collected before and after measurement. From chronoamperometry and impedance data, the Zn^{2+} transference number ($t_{Zn^{2+}}$) was calculated by the following equation:[3, 4]

$$t_{Zn^{2+}} = \frac{I_s(\Delta V - I_0 R_0)}{I_0(\Delta V - I_s R_s)},$$

Where ΔV is the applied constant polarization (10 mV), I_0 and R_0 are the initial current and resistance, and I_s and R_s are the steady-state current and resistance, respectively. Note that the resistances here refer to the charge transfer resistances.

Zn plating/striping

Symmetric Zn|Zn cells were assembled in coin cell configuration using Zn foil (φ=16mm) with glassy fiber (Whatman, GF/F) as the separator. The coin cells were tested on Neware battery testers, with constant current densities and capacities of 1 mA cm^{-2} and 1mAh cm^{-2}, 10 mA cm^{-2} and 10 mAh cm^{-2}, 50 mA cm^{-2} and 50 mAh cm^{-2}. To determine the Coulombic efficiencies (CEs) of electrolytes, asymmetric Ti|Zn cells were measured at 1 mA cm^{-2} and 1 mAh cm^{-2}.

AC/Zn full cell

The slurry was formulated by commercial AC (Kurary YP-80F), Super P (ECP-600JD) and PVDF in a weight ratio of 8:1:1. After casting and vacuum drying, the electrode on Ti mesh was with a mass loading of active material ~2 mg cm^{-2}. The coin cell was then assembled using the AC electrode (12 mm), ZCE-0 or ZCE-2, glassy fiber separator (19 mm), and the commercial Zn foil (16 mm) in CR2016 configuration. The galvanostatic charge/discharge curves were measured in the potential range of 0.3-1.9 V by Neware battery tester.

V_2O_5/Zn full cell

V_2O_5 nanosheets were synthesized by the previously reported process in large scale and the electrode preparation was conducted based on the previous report.[5] Briefly, the slurry was formulated by the synthesized V_2O_5 and Super P (TIMCAL) in a weight ratio of 8:2. After casting and vacuum drying, the binder-free electrode on stainless steel mesh was with a mass loading of active material ~1.5-2 mg cm^{-2}. The coin cells were assembled with 2M $Zn(OTf)_2$ as electroltye, and either commerial Zn or ZCE-Zn as anode. The galvanostatic charge/discharge curves were measured in the potential range of 0.3-1.8 V by Neware battery tester.

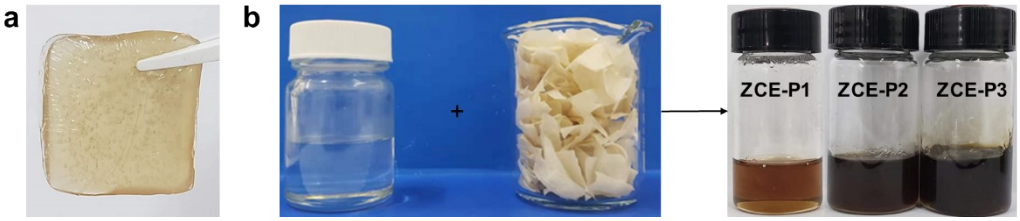

Figure S1. a) A regenerated cellulose film from ZCE-2 when soaked in excess ethanol. b) A series of complex electrolytes prepared by dissolving tissue paper in $ZnCl_2$ DES (i.e., ZCE-Px, x=1, 2, 3), following the same protocol as ZCEs.

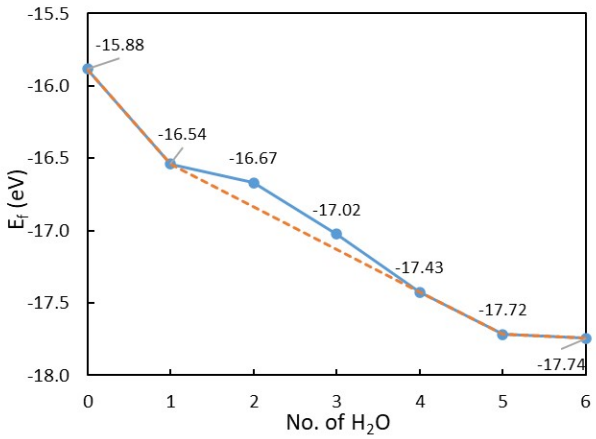

Figure S2. The formation energies E_f *vs.* the number of H_2O (n) for clusters $[Zn(OH_2)_n]^{2+} \cdot 2cellulose$.

Table S1. A summary of onset potentials of Zn/Zn^{2+} and OER, with the corresponding EW values for ZCEs.

Electrolyte	Onset potential of Zn deposition (V v.s. Zn/Zn^{2+})	OER (V v.s. Zn/Zn^{2+})	Electrochemical window (V)
ZCE-0	-0.03	1.96	1.99
ZCE-1	-0.02	1.95	1.97
ZCE-2	-0.03	3.29(8)	3.32
ZCE-3	-0.03	3.87	3.90

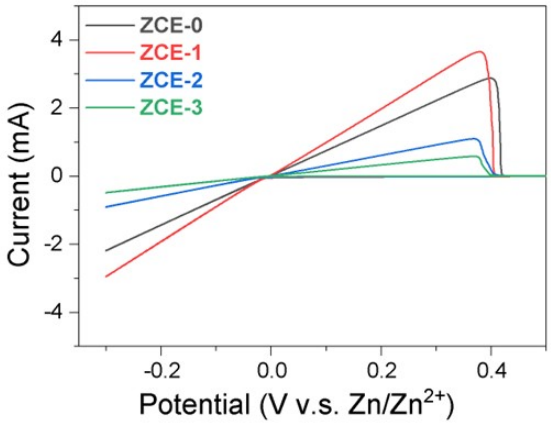

Figure S3. CV spectra of ZCEs showing the characteristics of Zn stripping/plating. The negative onset potentials of ZCEs from CV are consistent with the results from LSV, indicating the reduction potential of Zn. Stripping feature of deposited Zn was then followed by the positive scan. Following the discussion in Ref [6], CE was evaluated by asymmetric Ti|Zn cell under constant capacity and constant current mode.

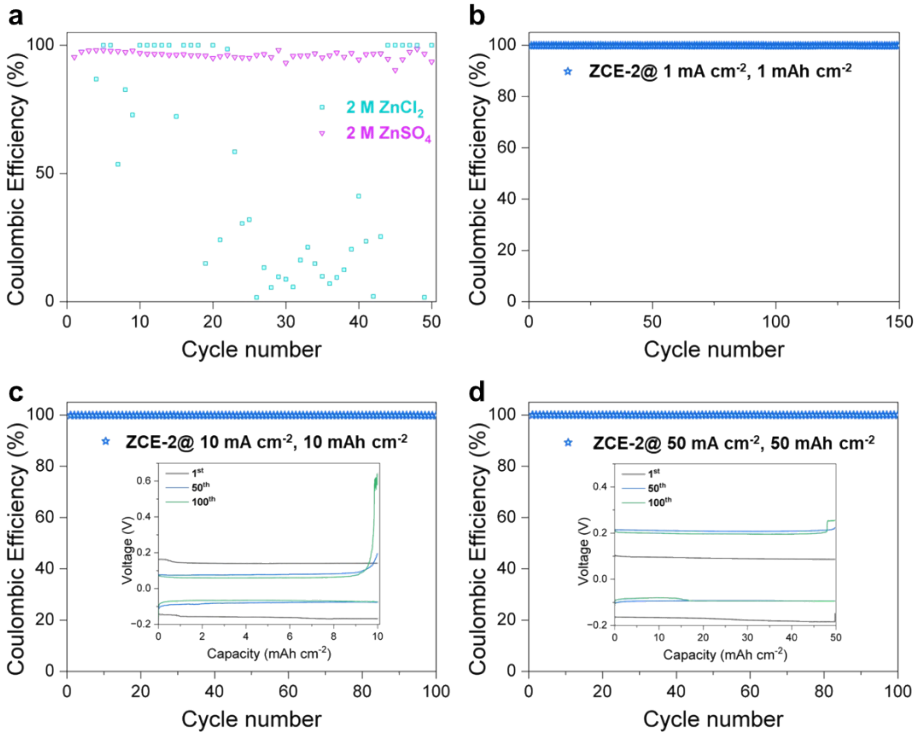

Figure S4. (a) Coulombic efficiencies (CEs) of Ti|Zn cells with 2 M $ZnCl_2$ and 2 M $ZnSO_4$ reference electrolytes. (b) CE for ZCE-2 for ZCE-2 at 1 mA cm^{-2} and 1 mAh cm^{-2} for 150 cycles, and (c) at 10 mA cm^{-2} and 10 mAh cm^{-2}, and (d) 50 mA cm^{-2} and 50 mAh cm^{-2}, where the insets present the polarization curves at 1st, 50th and 100th cycle, respectively.

Table S2. Summary of corrosion potentials and corrosion currents for the electrolytes.

Electrolyte	Corrosion potential (V v.s. Ag/AgCl)	Corrosion current ($mA \cdot cm^{-2}$)
2 M $ZnCl_2$	-0.940	3.01
ZCE-0	-0.658	0.29
ZCE-1	-0.658	0.23
ZCE-2	-0.650	0.19

a

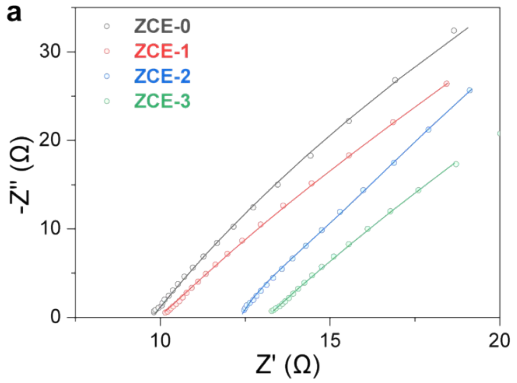

b

Electrolyte	σ by EIS (mS cm^{-1})	σ (mS cm^{-1})
ZCE-0	8.5	8.7
ZCE-1	8.0	8.1
ZCE-2	4.5	5.4
ZCE-3	3.9	4.4

Figure S5. (a) EIS spectra of symmetric cells of stainless steels to estimate the ionic conductivities of ZCEs. The estimation was based on $\sigma = \left(\frac{l}{S}\right)\frac{1}{R}$, where R is the contact resistance (Ω), S is taken to be 2.01 cm^2, and l is approximated to be 50 μm. And a contact resistance of 6.8 Ω has been corrected. (b) Summary of conductivities by EIS and conductivity meter.

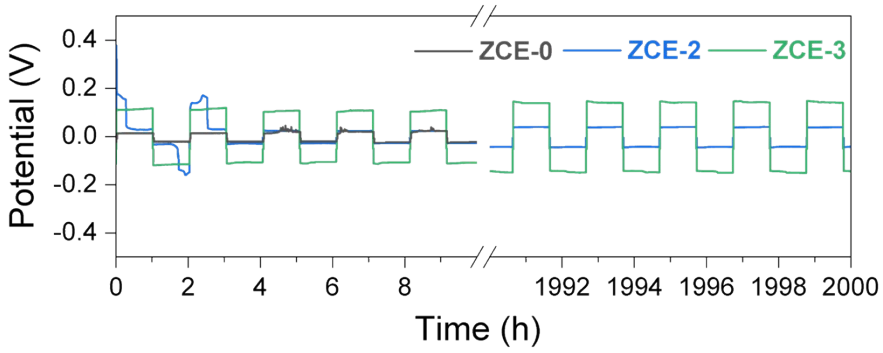

Figure S6. Voltage profiles comparing ZCE-0 and ZCE-2 at 10 mA cm^{-2} and 10 mAh cm^{-2}.

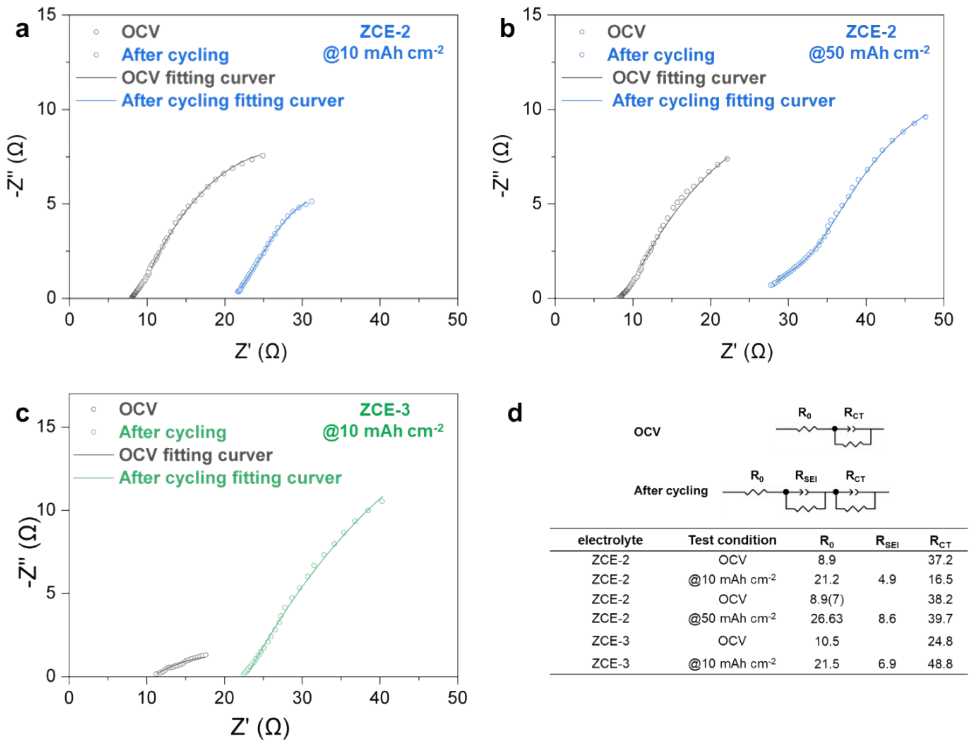

electrolyte	Test condition	R_0	R_{SEI}	R_{CT}
ZCE-2	OCV	8.9		37.2
ZCE-2	@10 mAh cm^{-2}	21.2	4.9	16.5
ZCE-2	OCV	8.9(7)		38.2
ZCE-2	@50 mAh cm^{-2}	26.63	8.6	39.7
ZCE-3	OCV	10.5		24.8
ZCE-3	@10 mAh cm^{-2}	21.5	6.9	48.8

Figure S7. EIS spectra of Zn|Zn before and after 200 cycles with ZCE-2 at (a) 10 mAh cm^{-2} and (b) 50 mAh cm^{-2}, and with ZCE-3 at (c) 10 mAh cm^{-2}, respectively. (d) Equivalent circuits for OCV and after cycling, with the fitted data for ZCE-2 and ZCE-3.

Table S3. DOD values for Zn in current $ZnCl_2$-based electrolytes, in Zn|Zn symmetric cells, which are typically below 6%.

Electrolyte	Working mode	Current density, Step capacity ($mA \cdot cm^{-2}$, $mAh \cdot cm^{-2}$)	Lifespan (h)	Zn foil thickness (mm)	Calculated DOD (%)	Reference
$ZnCl_2$:TMU:H_2O=1:3:1	constant current constant capacity	1, 1	2000	0.03	5.7	Adv. Funct. Mater. 2022, 2209065.
$ZnCl_2$:EG=1:4	constant current constant capacity	1, 1	3200	0.1	1.7	Angew. Chem. Int. Ed. 2022, 61, e202206717.
$ZnCl_2$:$Zn(OAc)_2$:H_2O=10:6:30.5	constant current constant capacity	0.2, 0.2	1000	0.08	0.42	Adv.Mater.2022, 34, 2201744.
7.6 m $ZnCl_2$+0.05 m $SnCl_2$	constant current constant capacity	3, 3	500	2.54	0.20	Angew. Chem. Int. Ed. 2021, 60, 18845.
$ZnCl_2$:DMSO:H_2O=1:34:7.9	constant current constant capacity	0.5, 0.5	1000	0.15 estimate	0.57	J. Am. Chem. Soc. 2020 142, 21404.
5 m $ZnCl_2$+5 m Betaine	constant current constant capacity	1, 1	900	0.15 estimate	1.1	Chem. Commun., 2022, 58, 8504–8507.
30 m $ZnCl_2$	constant current constant capacity	0.2, 0.033	600	0.15 estimate	1.4	Chem. Commun., 2018,54, 14097.
$ZnCl_2$:Ace:H_2O=1:3:1	constant current constant capacity	0.1, 0.1	1500	0.15 estimate	0.11	Adv. Funct. Mater. 2021, 31, 2102035.

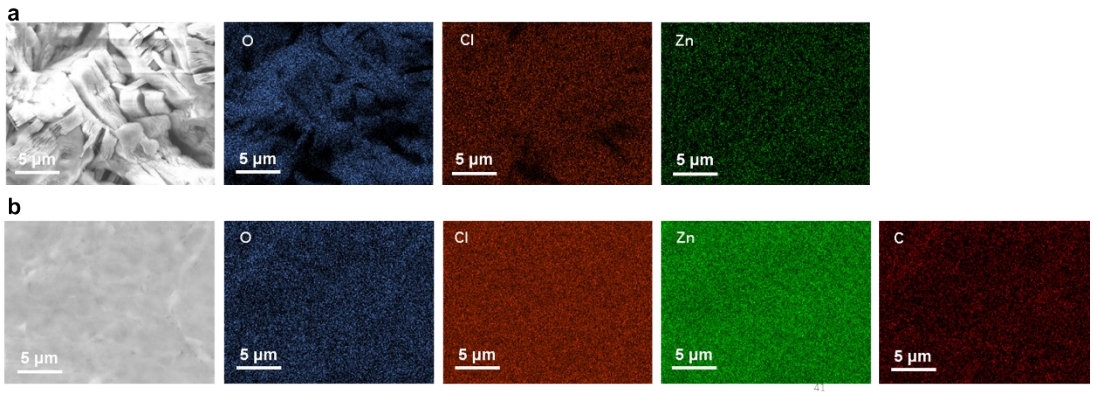

Figure S8. EDX mapping for the cycled Zn after stripping/plating in Zn|Zn symmetric cells for 1000 cycles with a) ZCE-0 and b) ZCE-2, respectively.

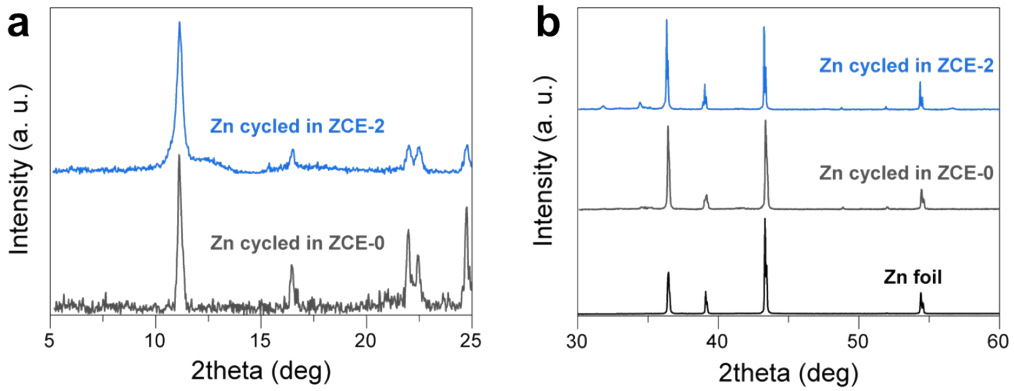

Figure S9. a) Grazing angle XRD patterns of Zn foils after stripping/plating in Zn|Zn symmetric cells for 1000 cycles with ZCE-0 and ZCE-2. b) XRD patterns comparing the intensity ratios of Zn (002)/(101), which are 0.44, 0.94, and 1.08 for Zn foil, cycled Zn in ZCE-0, and cycled Zn in ZCE-2, respectively.

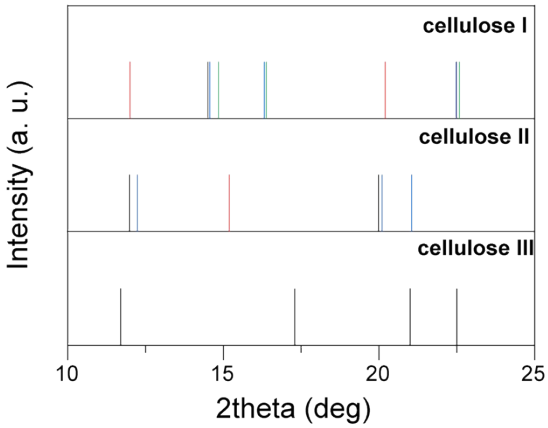

Figure S10. XRD patterns for the reported cellulose crystalline structures.[7-9]

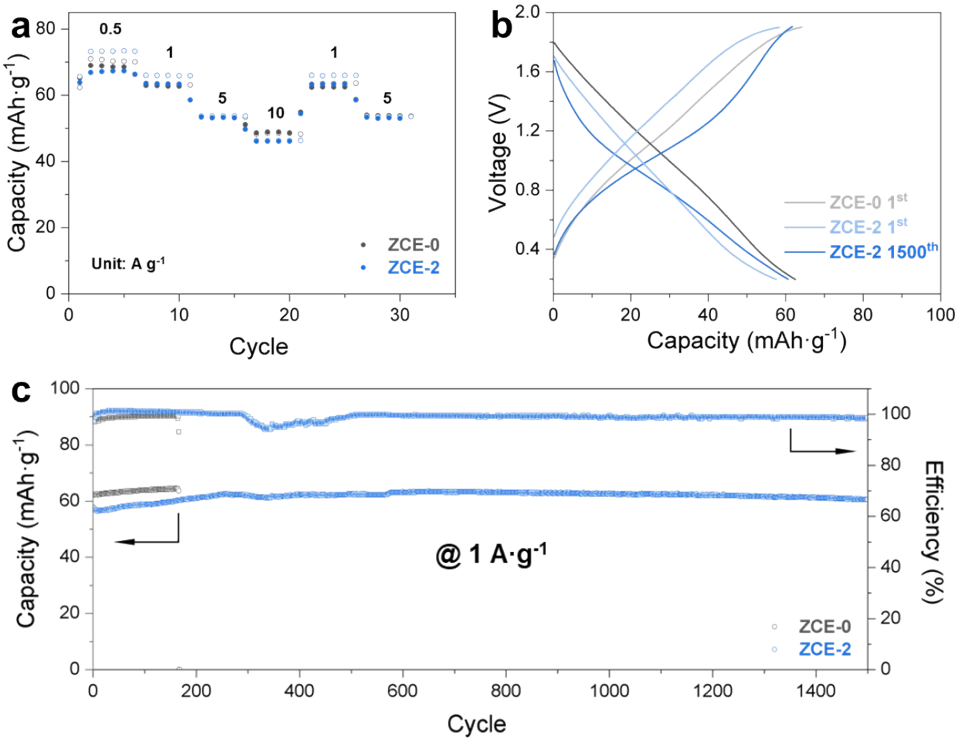

Figure S11. a) Rate performance of the AC/Zn cells with ZCE-2 and ZCE-0. AC/Zn cells comparing ZCE-0 and ZCE-2 at 1 A g^{-1} with b) charge/discharge curves and c) cycling performance.

At 1A g^{-1}, stable cycling with ZCE-2 can proceed for 1500 cycles, with an initial discharge capacity of ~57.8 mAh g^{-1} and ~60.6 mAh g^{-1} at 1500th cycle. This contrasts with only ~166 cycles with ZCE-0, where the short circuit is attributed to Zn dendrite growth.

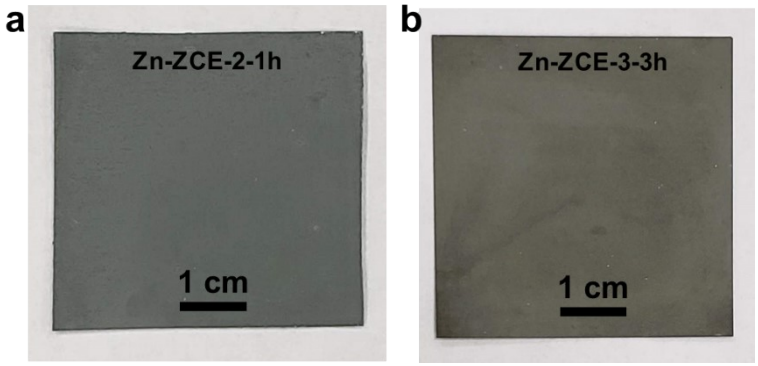

Figure S12. Optical images of a) Zn-ZCE-2-1h and b) Zn-ZCE-3-3h.

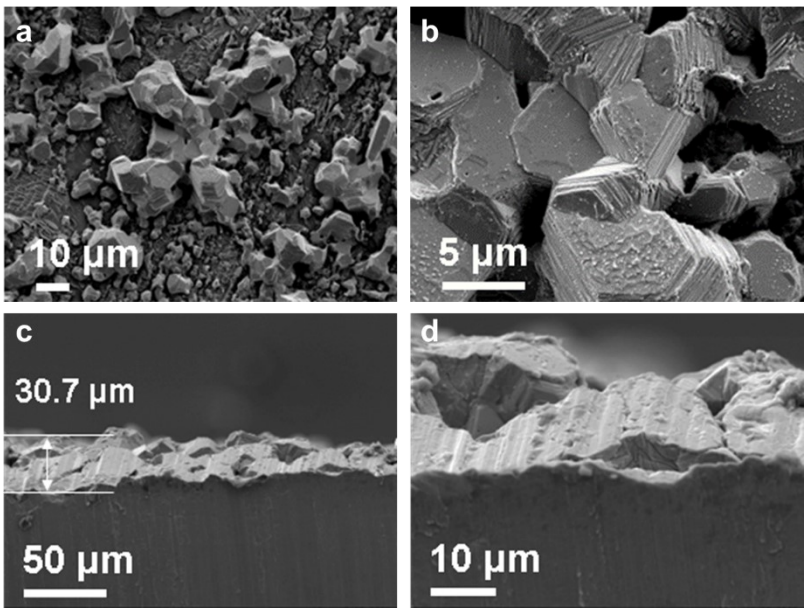

Figure S13. SEM images of Zn-ZCE-0-1h with a) in-plane view with b) the magnified view, and c) cross section view with d) the magnified view where a deposited layer of ~30.7 µm can be observed.

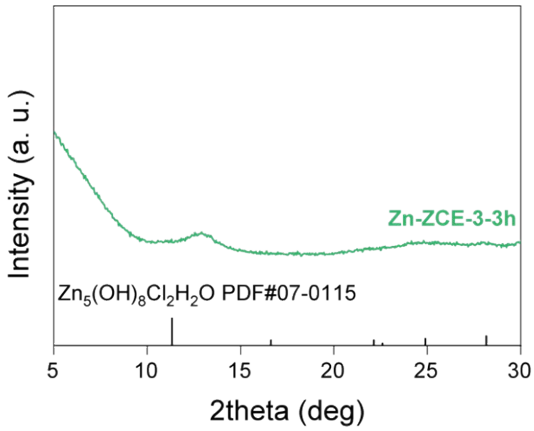

Figure S14. XRD pattern of the deposited surface by ZCE-3 for 3h (Zn-ZCE-3-3h), presenting the broad diffraction peak at ~12.9°.

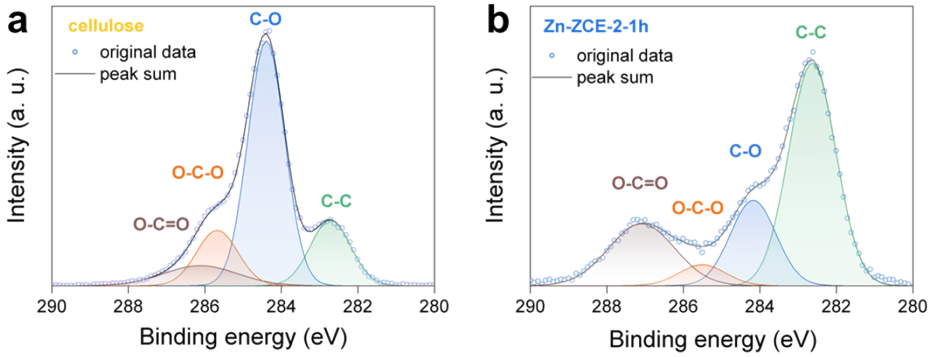

Figure S15. XPS spectra of C1*s* for a) cellulose and b) Zn-ZCE-2-1h.

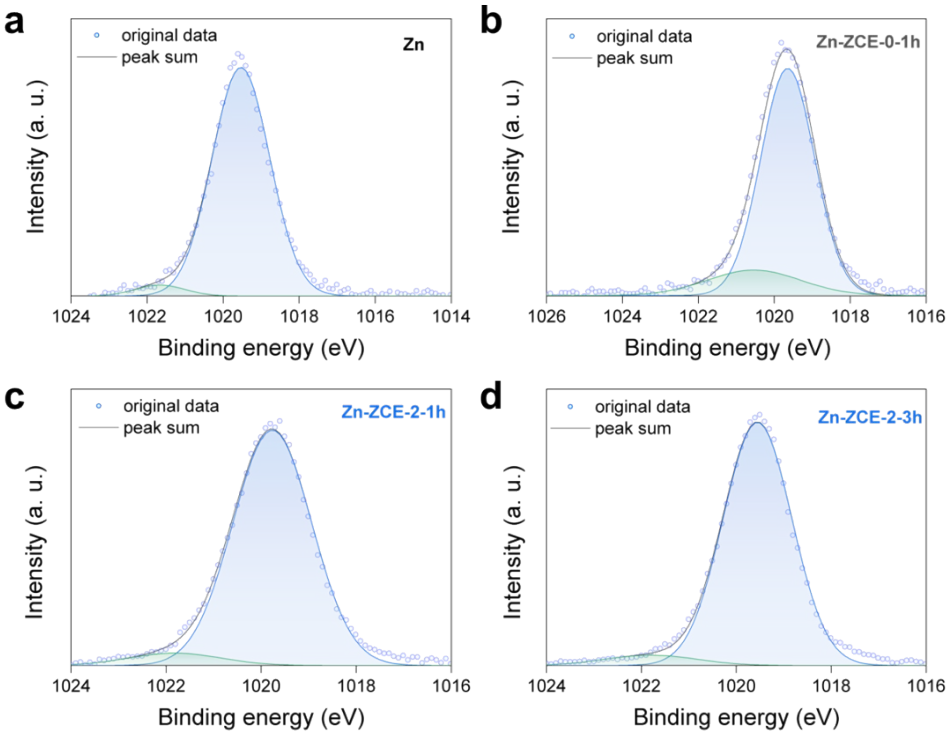

Figure S16. XPS spectra of Zn 2p for a) bare Zn, b) Zn-ZCE-0-1h, c) Zn-ZCE-Zn-1h, and d) Zn-ZCE-Zn-3h, respectively, where the deconvoluted peaks are assigned to Zn^0 and Zn-O accordingly.[10]

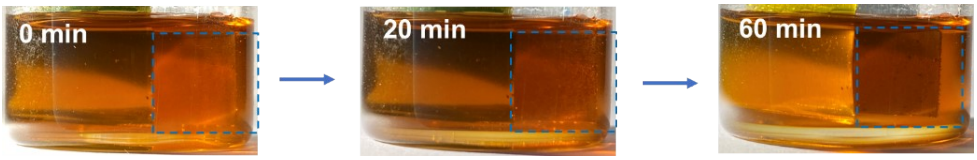

Figure S17. Time-dependent study of ZCE growth on Zn, where the SEI formation was observed on the electrode during deposition.

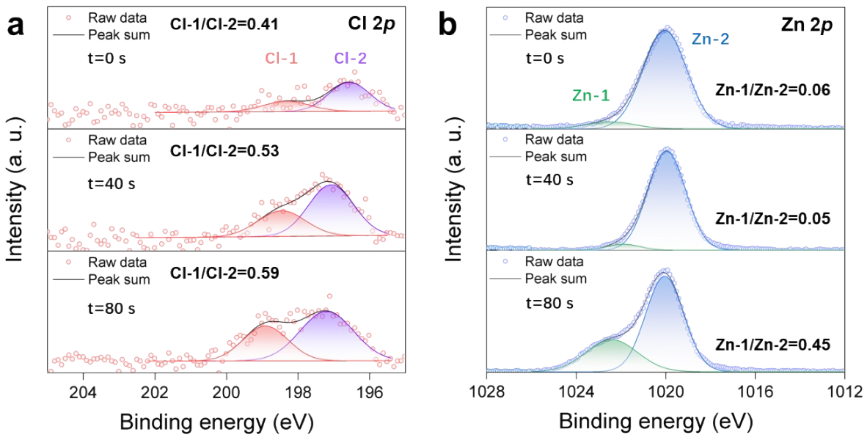

Figure S18. XPS depth profile for the artificial SEI on Zn concerning (a) Cl 2p and (b) Zn 2p, with a step sputtering depth of ~8 nm.

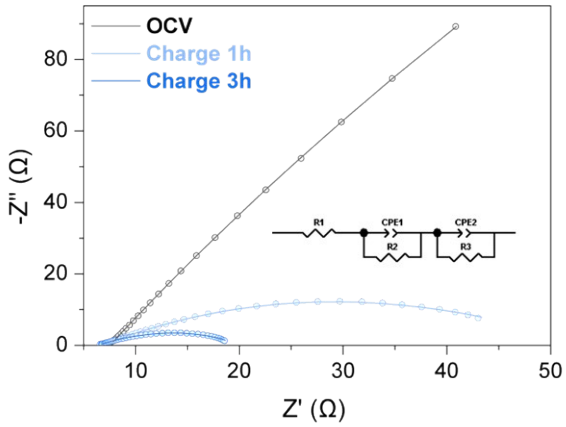

Figure S19. Real-time EIS spectra to study the effects of deposited layer on interface kinetics. It shows that R_{CT} decreases from 1799 Ω at OCV, to 35 Ω for ZCE-Zn-1h when the interface is growing, and further to 11 Ω for ZCE-Zn-3h.

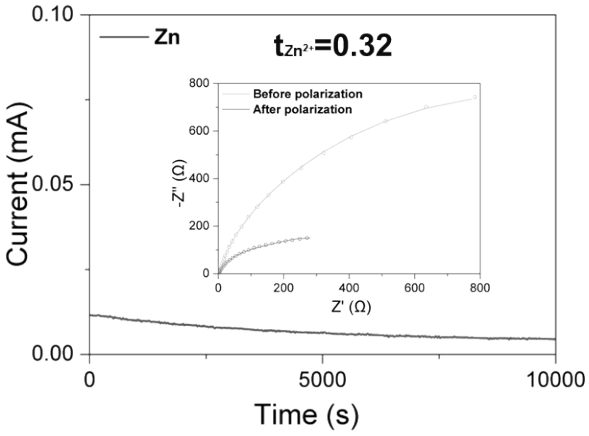

Figure S20. Transference number for the cell with bare Zn in 2M $Zn(OTf)_2$, where the inset presents the EIS spectra before and after polarization.

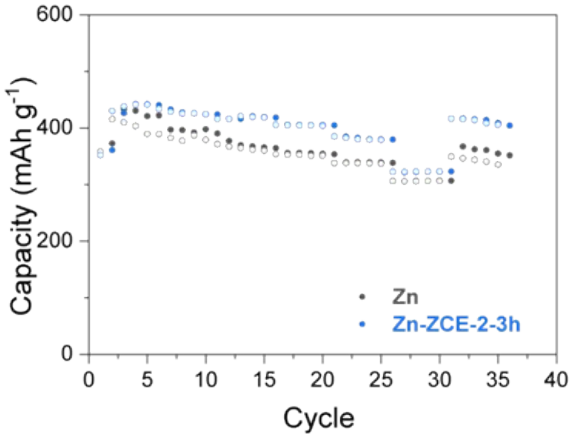

Figure S21. Rate performance of the V_2O_5 based full cells, comparing Zn-ZCE-2-3h and Zn.

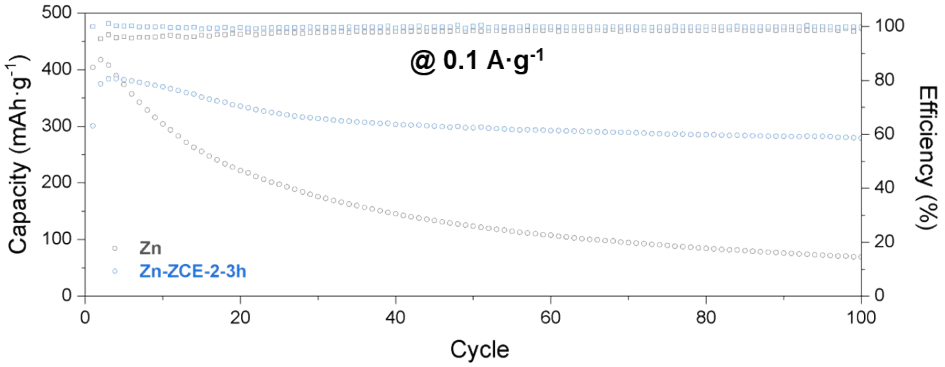

Figure S22. Cycling stability comparing V_2O_5/Zn and V_2O_5/Zn-ZCE-2-3h cells at 0.1 A g^{-1}.

References

1. M. J. Frisch, G. W. Trucks, H. B. Schlegel, G. E. Scuseria, M. A. Robb, J. R. Cheeseman, G. Scalmani, V. Barone, G. A. Petersson, H. Nakatsuji, X. Li, M. Caricato, A. V. Marenich, J. Bloino, B. G. Janesko, R. Gomperts, B. Mennucci, H. P. Hratchian, J. V. Ortiz, A. F. Izmaylov, J. L. Sonnenberg, Williams, F. Ding, F. Lipparini, F. Egidi, J. Goings, B. Peng, A. Petrone, T. Henderson, D. Ranasinghe, V. G. Zakrzewski, J. Gao, N. Rega, G. Zheng, W. Liang, M. Hada, M. Ehara, K. Toyota, R. Fukuda, J. Hasegawa, M. Ishida, T. Nakajima, Y. Honda, O. Kitao, H. Nakai, T. Vreven, K. Throssell, J. A. Montgomery Jr., J. E. Peralta, F. Ogliaro, M. J. Bearpark, J. J. Heyd, E. N. Brothers, K. N. Kudin, V. N. Staroverov, T. A. Keith, R. Kobayashi, J. Normand, K. Raghavachari, A. P. Rendell, J. C. Burant, S. S. Iyengar, J. Tomasi, M. Cossi, J. M. Millam, M. Klene, C. Adamo, R. Cammi, J. W. Ochterski, R. L. Martin, K. Morokuma, O. Farkas, J. B. Foresman and D. J. Fox, *Journal*, 2016.
2. Y. Zhao and D. G. Truhlar, *Theoretical Chemistry Accounts*, 2008, **120**, 215-241.
3. J. Evans, C. A. Vincent and P. G. Bruce, *Polymer*, 1987, **28**, 2324-2328.
4. F. Wu, N. Chen, R. Chen, Q. Zhu, J. Qian and L. Li, *Chemistry of Materials*, 2016, **28**, 848-856.
5. J. Zhao, H. Ren, Q. Liang, D. Yuan, S. Xi, C. Wu, W. Manalastas, J. Ma, W. Fang, Y. Zheng, C.-F. Du, M. Srinivasan and Q. Yan, *Nano Energy*, 2019, **62**, 94-102.
6. L. Ma, M. A. Schroeder, O. Borodin, T. P. Pollard, M. S. Ding, C. Wang and K. Xu, *Nature Energy*, 2020, **5**, 743-749.
7. A. D. French, *Cellulose*, 2014, **21**, 885-896.
8. X.-F. Zhang, T. Hou, J. Chen, Y. Feng, B. Li, X. Gu, M. He and J. Yao, *ACS Applied Materials & Interfaces*, 2018, **10**, 24930-24936.
9. Q. Zhu, X. Zhou, J. Ma and X. Liu, *Industrial & Engineering Chemistry Research*, 2013, **52**, 17900-17906.
10. D. Yuan, W. Manalastas Jr, L. Zhang, J. J. Chan, S. Meng, Y. Chen and M. Srinivasan, *ChemSusChem*, 2019, **12**, 4889-4900.